Heliyon 9 (2023) e20650

Contents lists available at ScienceDirect

Heliyon

journal homepage: www.cell.com/heliyon

Derepressing of STAT3 and USP7 contributes to resistance of DLBCL to EZH2 inhibition

Chenyun He [a], Wenbin Zhou [b], Xiaoxia Jin [a], Haining Zhou [c,*]

[a] *Affililated Tumor Hospital of Nantong University, Nantong, Jiangsu, China*
[b] *East Hospital of Shaoyang Central Hospital Medical Group, Shaoyang, Hunan, China*
[c] *National Laboratory of Biomacromolecules, Institute of Biophysics, Chinese Academy of Sciences, Beijing, China*

A B S T R A C T

Diffuse large B-cell lymphoma is the most common subtype of lymphoma, representing ~25 % of non-Hodgkin lymphoid malignancies. EZH2 is highly expressed in Diffuse large B-cell lymphoma and ~22 % of patients contain EZH2 mutations. EZH2 have been studied as a potential therapeutic target for a decade, but efficient inhibition of EZH2 did not robustly kill lymphoma cells. Here, we found that EZH2 mediates repression of oncogenic genes *STAT3* and *USP7* in Diffuse large B-cell lymphoma cells. Inhibition of EZH2 leads to upregulation of STAT3 and USP7 at both RNA and protein levels. Along with USP7 upregulation, MDM2 is upregulated and its ubiquitylation substrate, Tumor suppressor P53, is downregulated. Upregulation of STAT3 and downregulation of p53 can strength cell proliferation and prevent cells from apoptosis, which suggests resistance mechanisms by which cells survive EZH2 inhibition-induced cell death. Short-course co-inhibition of USP7 and EZH2 showed increased apoptosis and cell proliferation prevention with the concentration as low as 0.08 μM. In STAT3 and USP7 depleted cells, EZH2 inhibition shows superior efficacy of apoptosis, and in EZH2 depleted cells, USP7 inhibition also shows superior efficacy of apoptosis. Thus, our findings suggest a new precision therapy by combinational inhibition of EZH2 with STAT3 or USP7 for Diffuse large B-cell lymphoma.

1. Introduction

Polycomb Repressive Complex (PRC) PRC1 and PRC2, and the histone modifications H3K27me3 (Histone H3 lysine 27 trimethylation) and H2AK119ub1 (Histone H2A lysine 119 mono-ubiquitylation) consist of polycomb repressive system that mediates transcriptional repression of cell differentiation and cell proliferation associated genes [1,2]. The Histone methyltransferase EZH2 is a subunit of PRC2 and stably binds to the other two PRC2 core components EED and SUZ12, and EZH2 catalyzes mono-, di-, and tri-methylation at lysine 27 of Histone H3 (H3K27me1, H3K27me2, and H3K27me3), of which H3K27me3 is a repressive Histone mark that is mainly deposited at promoter regions [2,3]. PRC1 recognizes and binds to the Histone H3 tail harboring this mark. H3K27me3-dependent accumulation of PRC1 at promoter regions mediate transcriptional repression involving mechanisms including chromatin compaction, nascent RNA processing, HDACs recruitment, liquid-liquid phase separation, and/or so on [2,4].

Polycomb is essential for regulating B cell differentiation. In the transition from Naïve B cells to germinal B cells [5,6], EZH2 expression level spikes and leads to repression of proliferation checkpoint genes like CDKN1A and differentiation genes PRDM1 (plasma cell differentiation), and IRF4 (terminal germinal center B cell differentiation) [6–8], and transiently suppresses germinal center B cell differentiation to allow for immunoglobulin somatic hypermutation [5]. EZH2 has also been shown highly expressed and frequently mutated in germinal center B-cell subtype of Diffuse large B-cell lymphoma (GCB DLBCL, ~22 % mutation) and follicular lymphoma (FL, ~17%mutation) [9–14], and a large subset of them contains gain-of-function mutations in the catalytic domain of

* Corresponding author.
E-mail address: zhouhaining@ibp.ac.cn (H. Zhou).

https://doi.org/10.1016/j.heliyon.2023.e20650
Received 11 October 2022; Received in revised form 22 September 2023; Accepted 3 October 2023
Available online 5 October 2023
2405-8440/© 2023 The Authors. Published by Elsevier Ltd. This is an open access article under the CC BY-NC-ND license (http://creativecommons.org/licenses/by-nc-nd/4.0/).

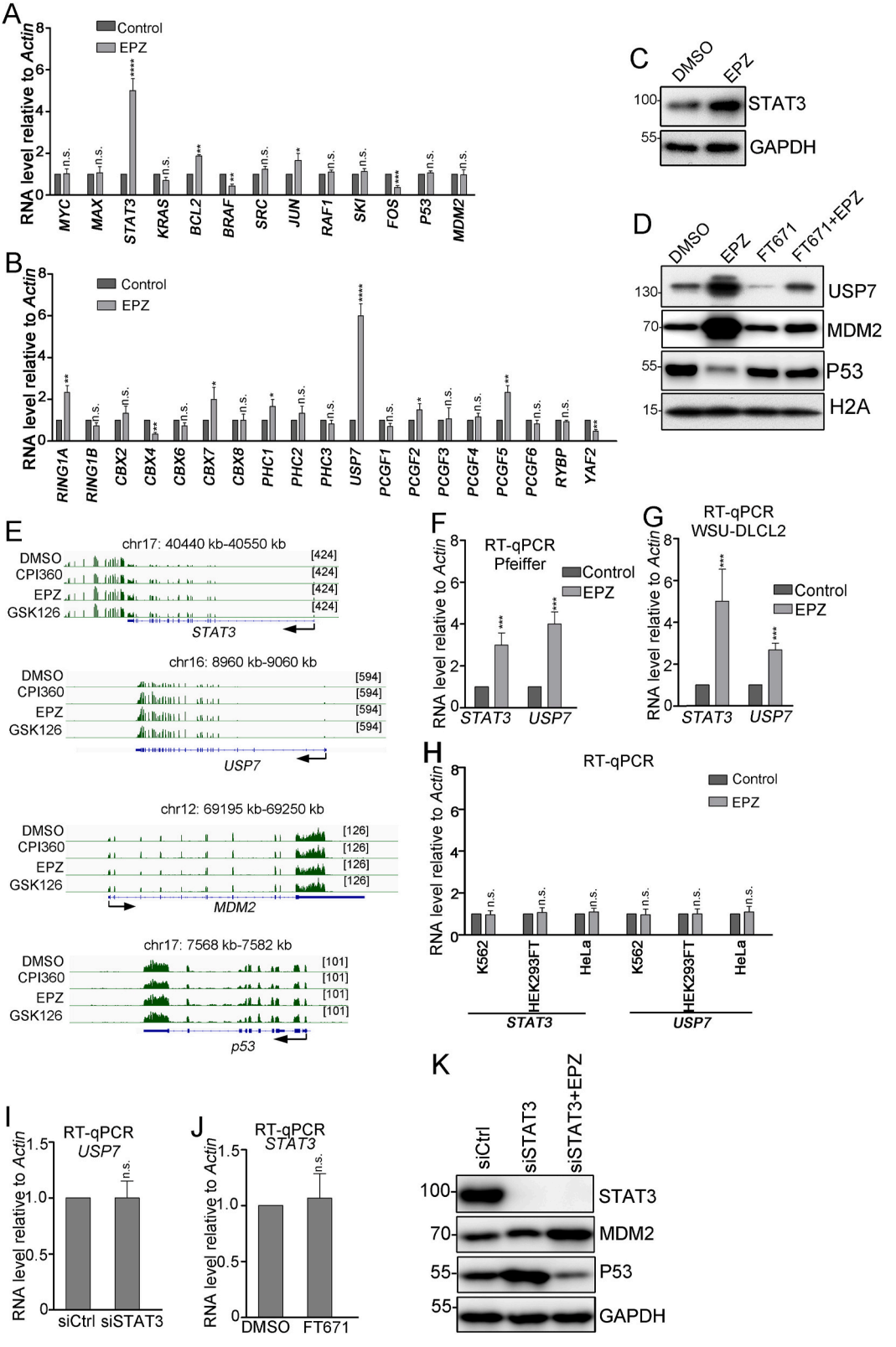

(caption on next page)

Fig. 1. STAT3 and USP7 are upregulated in EZH2 treated DLBCL cells.
A. RT-qPCR analysis of RNA levels for the indicated oncogenic genes in DMSO or EPZ (1 μM) treated KARPAS-422 cells for 3 days. RNA expression levels were normalized to *ACTB*. Error bars represent standard deviations for three biological replicates. P value is from two-sided student's t-test. n. s., not significant; *p < 0.05; **p < 0.01; ***p < 0.001; ****p < 0.0001.
B. RT-qPCR analysis of RNA levels for the indicated PRC1 subunits in DMSO or EPZ (1 μM) treated KARPAS-422 cells for 3 days. RNA expression levels were normalized to *ACTB*. Error bars represent standard deviations for three biological replicates. P value is from two-sided student's t-test. n. s., not significant; *p < 0.05; **p < 0.01; ****p < 0.0001.
C. Immunoblotting showing STAT3 protein abundance in DMSO or EPZ (1 μM) treated KARPAS-422 cells for 3 days. GAPDH served as loading control.
D. Immunoblotting showing indicated protein abundance in DMSO or EPZ (1 μM) treated KARPAS-422 cells for 3 days. H2A served as loading control.
E. Genomic snapshots of RNA-seq reads at *STAT3, USP7, MDM2,* and *P53* in KARPAS-422 cells with DMSO (GSM1519048), CPI360 (1.5 μM, GSM1519050), EPZ (1.5 μM, GSM1519052), and GSK126 (1.5 μM, GSM1519054) treated cells for 4 days. Enrichment levels (log2) were normalized with Reads Per Genome Coverage.
F. RT-qPCR analysis of RNA levels for STAT3 and USP7 in DMSO or EPZ (1 μM) treated Pfeiffer cells for 3 days. RNA expression levels were normalized to *ACTB*. Error bars represent standard deviations for three biological replicates. P value is from two-sided student's t-test. **p < 0.01; ***p < 0.001.
G. RT-qPCR analysis of RNA levels for STAT3 and USP7 in DMSO or EPZ (1 μM) treated WSU-DLCL2 cells for 3 days. RNA expression levels were normalized to *ACTB*. Error bars represent standard deviations for three biological replicates. P value is from two-sided student's t-test. ***p < 0.001.
H. RT-qPCR analysis of RNA levels for STAT3 and USP7 in DMSO or EPZ (1 μM) treated K562, HEK293FT, and HeLa cells for 3 days. RNA expression levels were normalized to *ACTB*. Error bars represent standard deviations for three biological replicates. P value is from two-sided student's t-test. n. s., not significant.
I. RT-qPCR analysis of RNA levels for USP7 in control or STAT3 siRNA treated KARPAS-422 cells for 3 days. RNA expression levels were normalized to *ACTB*. Error bars represent standard deviations for three biological replicates. P value is from two-sided student's t-test. n.s., not significant.
J. RT-qPCR analysis of RNA levels for STAT3 in DMSO or FT671 (1 μM) treated KARPAS-422 cells for 3 days. RNA expression levels were normalized to *ACTB*. Error bars represent standard deviations for three biological replicates. P value is from two-sided student's t-test. n.s., not significant.
K. Immunoblotting showing indicated protein abundance in siControl, siSTAT3, or siSTAT3+EPZ (1 μM) treated KARPAS-422 cells for 3 days. GAPDH served as loading control.
For uncropped images, please see supplementary file 1.

EZH2 and this leads to increased promoter H3K27me3[[6,13]]. Mutant EZH2 aberrantly represses genes through increased H3K27me3 and potentially more recruitment of PRC1 to chromatin, which more strongly blocks cell differentiation than WT EZH2 and contributes to germinal center hyperplasia and lymphomagenesis [6].

EZH2, as a therapeutic target, has been under intense investigation for curing DLBCL and FL. Several promising small molecules have been identified and under clinic trials [15]. The oncogenic roles are also proposed in several other lymphoma subtypes, such as mantle cell lymphoma and T cell lymphoma [16,17]. Tazemetostat (also known as EPZ-6438, this paper we call it EPZ) was approved by US Food and Drug Administration in relapsed/refractory FL [18,19]. There are several ongoing clinical trials on DLBCL and FL, but single treatment with EZH2 inhibitors in DLBCL is modest in efficacy [20], and in vitro long-term treatment cultured cells induced gain of secondary mutations on EZH2 (e.g. Y111L, Y661D, C663Y, and Y726F) and resistance to drugs[[19,21,22]].This led us to ask why EZH2 inhibition in DLBCL is not toxically strong enough, and if there is adapted mechanisms by which lymphoma cell survive EZH2 inhibition. Long-term inhibition induced acquired mutations on EZH2 also indicates that rapid cell death upon treatment is important for further therapy approach development.

2. Results

STAT3 and USP7 are upregulated at both RNA and protein levels in response to EZH2 inhibition.

To address the questions that if there is resistance mechanism by which DLBCL cells tolerate EZH2 inhibitor treatment, we used EPZ to treat KARPAS-422 cells for 3 days and examined 11 oncogenic genes *MYC, MAX, STAT3, KRAS, BCL2, BRAF, SRC, JUN, RAF1, SKI, FOS, MDM2*, and a tumor suppression factor *p53*. *STAT3* was highly upregulated upon EZH2 inhibition by ~5 fold (Fig. 1A). *P53*, apoptosis inducing factor, was not significantly changed but one of its upstream regulators USP7 is upregulates by ~6-fold (Fig. 1B). By ubiquitylation of p53, MDM2 promotes degradation of p53, and USP7 downregulates p53 by deubiquitylating and protecting MDM2 from degradation [23,24]. USP7 is also shown to be a subunit of PRC1, which colocalize and collaborates with PRC2 to repress gene expression [2]. To examine if EZH2 can regulate PRC1 expression, we checked all the other PRC1 subunits RNA levels. Most of them were not upregulated, except for *RING1A*, *PCGF5* and *CBX7* (upregulated by ~2-fold) (Fig. 1B). Consistent with RNA-level upregulation, STAT3 and USP7 proteins were also significantly increased (Fig. 1C-D). USP7 inhibition induces reduction of USP7 proteins (Fig. 1D), suggesting catalytically inhibited USP7 proteins tend to be degraded. MDM2 is also upregulated in EPZ-treated cells (Fig. 1D). Different from USP7 and MDM2, p53 is largely downregulated in EPZ-treated cells (Fig. 1D). Consistently, by checking published RNA-seq data, *USP7* and *STAT3* were shown upregulated in KARPAS-422 cells with treatment of three different EZH2 inhibitors (CPI360, EPZ, and GSK126), but *MDM2* and *p53* RNA levels were not significantly changed, indicating MDM2 and p53 were regulated at protein levels by USP7 [25] (Fig. 1E). We further tested two additional DLBCL cell lines (Pfeiffer and WSU-DLCL2) and three other no-lymphoma cell types (K562, HEK293FT, and HeLa). *STAT3* and *USP7* were upregulated in Pfeiffer and WSU-DLCL2 cells upon EPZ treatments but not in K562, HEK293FT, and HeLa cells (Fig. 1F–H). Knockdown of STAT3 did not significantly affect *USP7*

expression and inhibition of USP7 also didn't greatly change STAT3 expression, suggesting STAT3 and USP7 are independently regulated in DLBCL cells (Fig. 1I-J). While STAT3 negatively regulated p53 protein level indicating its role in preventing cell apoptosis (Fig. 1K). Although DLBCL is highly heterogenous, the results in three cell lines (KARPAS-422, Pfeiffer and WSU-DLCL2) indicate that at least a subset of DLBCL patients can respond to EZH2 inhibition by increasing STAT3 and USP7.

2.1. PRC1/2 represses STAT3 and USP7

To examine how STAT3 and USP7 were upregulated in EZH2 inhibited cells mechanistically, we analyzed H3K27me3 ChIP-seq data and looked at distribution of Histone mark H3K27me3 that is catalyzed by PRC2 in three DLBCL cells lines (KARPAS-422, Pfeiffer and WSU-DLCL2) and three other cell lines (K562, HeLa, and HEK293FT). H3K27me3 was shown to be enriched at promoter regions of both *STAT3* and *USP7* in all the three DLBCL cell lines but not the others (Fig. 2A). H3K27me3 is spread to gene body of *STAT3* in Karpas-422 and WSU-DLCL2 cells and spread to gene body of *USP7* in KARPAS-422 and Pfeiffer cells (Fig. 2A). To examine why H3K27me3 specifically targets *STAT3* and *USP7* in DLBCL cells, we checked expression levels of several components of PRC1 (RING1A, RING1B, USP7, and CBX2) and PRC2 (EZH2), and histone mark H2AK119ub1 (catalyzed by PRC1) and H3K27me3

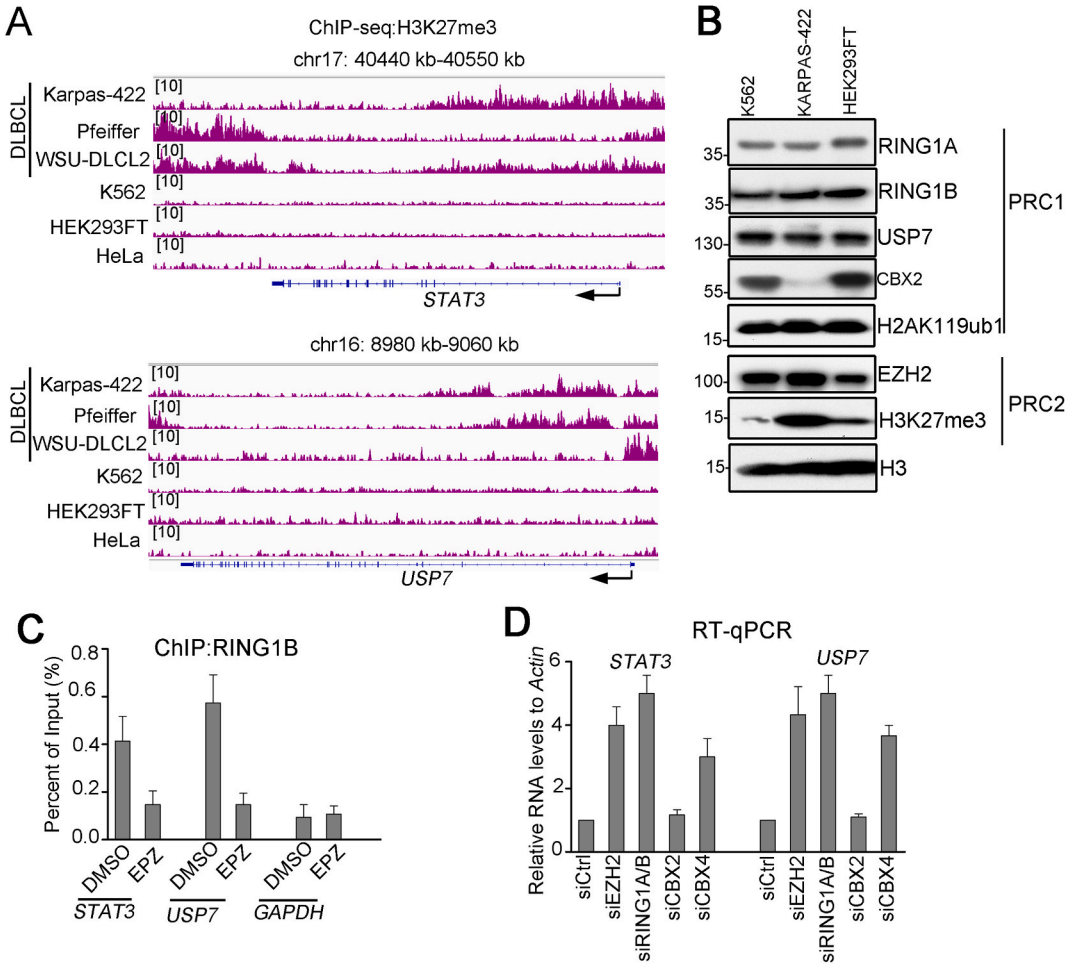

Fig. 2. STAT3 and USP7 are targets of polycomb in DLBCL cells KARPAS-422, Pfeiffer, and WSU-DLCL2.

A. Genomic snapshots of H3K27me3 ChIP-seq reads at *STAT3* and *USP7* for the indicated cell types. Enrichment levels (log2) were normalized with Reads Per Genome Coverage.KARPAS-422,GSM1006151; Pfeiffer, GSM1006149; WSU-DLCL2, GSM1006154; K562, GSM1782739; HEK293FT, GSM4239945; HeLa, GSM5343693.

B. Immunoblotting showing indicated protein abundance and H3K27me3 and H2AK119ub1 levels in wild type K562, KARPAS-422, and HEK293FT cells. H3 served as loading control.

C. ChIP-qPCR experiments showing the localization of RING1B at the indicated genes in DMSO or EPZ (1 μM) treated KARPAS-422 cells for 3 days. *GAPDH* served as a control. Error bars represent standard deviations for three biological replicates.

D. RT-qPCR analysis of RNA levels for *STAT3* and *USP7* in the indicated siRNA-treated KARPAS-422 cells for 3 days. RNA expression levels were normalized to *ACTB*. Error bars represent standard deviations for three biological replicates.

For uncropped image, please see supplementary file 2.

(catalyzed by PRC2) by immunoblotting in K562, KARPAS-422 and HEK293FT. Most PRC1 subunits were at similar levels in three cell lines as well as H2AK119ub1, except for CBX2, which is lowly expressed in KARPAS-422 (Fig. 2B). However, EZH2 protein level is higher in KARPAS-422 than in K562 and HEK293FT, which is consistent with literature that EZH2 was highly expressed in lymphoma[[6,13,16]]. The bulk abundance of H3K27me3 is much higher in KARPAS-422, suggesting that EZH2/PRC2 is catalytically hyperactive in the cells (Fig. 2B). This hyperactivity may explain why we observe euchromatic genes *STAT3* and *USP7* were decorated with heterochromatic mark H3K27me3 in DLBCL cells.

Polycomb mediated gene repression has involved both PRC1 and PRC2. PRC1 subunits CBX2/4/6/7/8 can recognize and bind H3 tail with H3K27me3 and accumulated PRC1 further catalyzes H2AK119ub1 and mediates transcriptional repression [2]. To address if

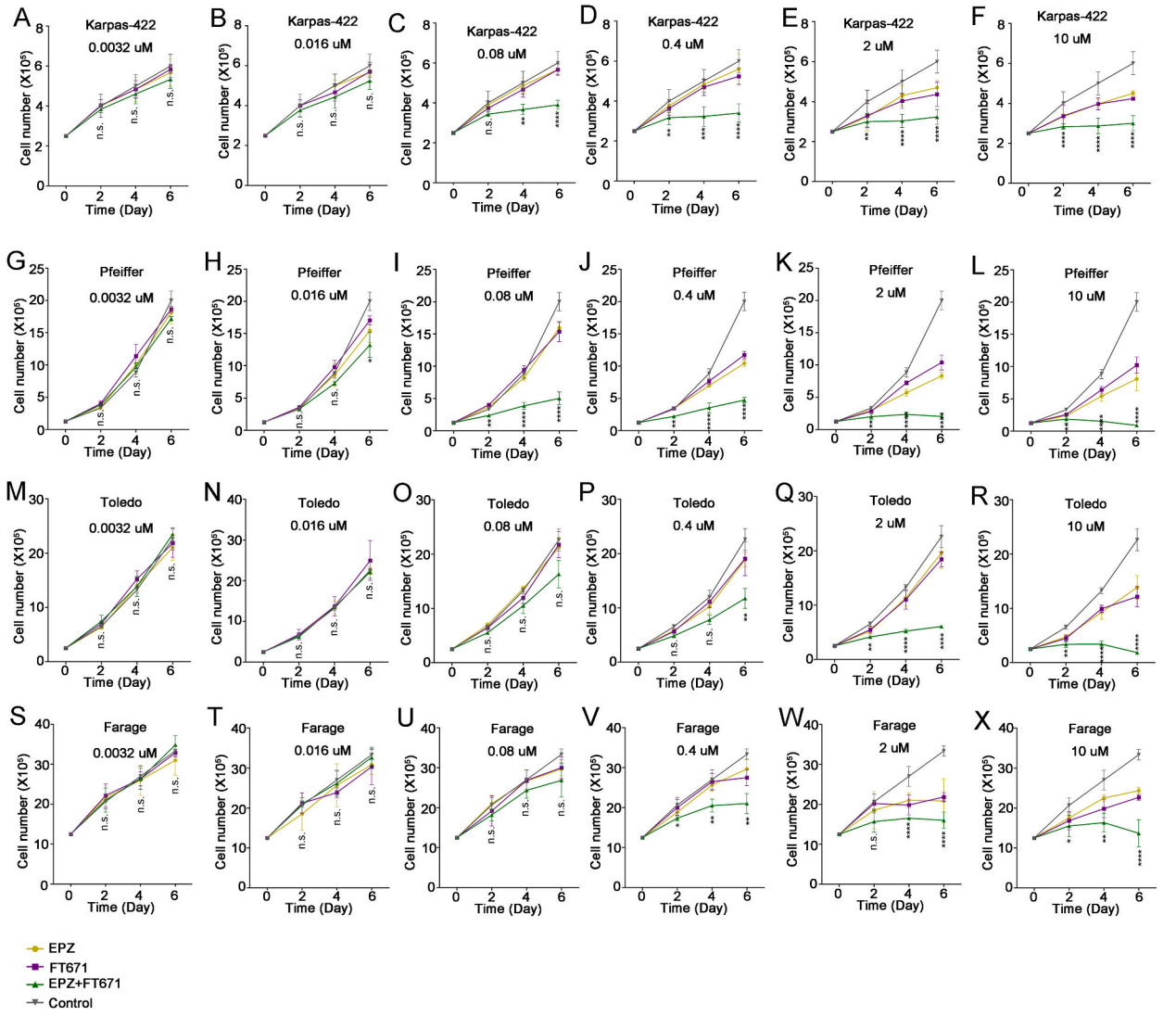

Fig. 3. Combinational inhibition of EZH2 and USP7 prevent cell proliferation at low concentration.

A-F. Growth curves show cell number changes at indicated time points after treatment of indicated drugs to KARPAS-422 cells. The drug concentrations were 0.0032 μM (A), 0.016 μM (B), 0.08 μM (C), 0.4 μM (D), 2 μM (E), 10 μM (F). Error bars represent standard deviation for three biological replicates.

G-L. Growth curves show cell number changes at indicated time points after treatment of indicated drugs to Pfeiffer cells. The drug concentrations were 0.0032 μM (G), 0.016 μM (H), 0.08 μM (I), 0.4 μM (J), 2 μM (K), 10 μM (L). Error bars represent standard deviation for three biological replicates. From A-L, P value is from two-sided student's t-test. n.s., not significant; *p < 0.05; **p < 0.01; ***p < 0.001; ****p < 0.0001.

M-R. Growth curves show cell number changes at indicated time points after treatment of indicated drugs to Toledo cells. The drug concentrations were 0.0032 μM (M), 0.016 μM (N), 0.08 μM (O), 0.4 μM (P), 2 μM (Q), 10 μM (R). Error bars represent standard deviation for three biological replicates. From A-L, P value is from two-sided student's t-test. n.s., not significant; **p < 0.01; ****p < 0.0001.

S-X. Growth curves show cell number changes at indicated time points after treatment of indicated drugs to Farage cells. The drug concentrations were 0.0032 μM (S), 0.016 μM (T), 0.08 μM (U), 0.4 μM (V), 2 μM (W), 10 μM (X). Error bars represent standard deviation for three biological replicates. From A-L, P value is from two-sided student's t-test. n.s., not significant; *p < 0.05; **p < 0.01; ****p < 0.0001.

STAT3 and USP7 are repressed by PRC1, we performed ChIP-qPCR of RING1B, which is a catalytic subunit of PRC1. We observed enrichment of RING1B at *STAT3* and *USP7* compared to housekeeping gene *GAPDH* (Fig. 2C). and the enrichment of RING1B was reduced in EZH2 inhibited cells, suggesting PRC1 is recruited to *STAT3* and *USP7* by EZH2 catalyzed H3K27me3 (Fig. 2C). Further siRNA-mediated knockdown (KD) and followed qPCR assays showed RING1B and CBX4 KD induce upregulation of *STAT3* and *USP7*, which is similar with EZH2 KD. CBX2 KD didn't show an increase, suggesting CBX4, instead of CBX2, dominates PRC1 function in this cell line, which correlated with low protein expression level of CBX2 in KARPAS-422 cells (Fig. 2B and D).

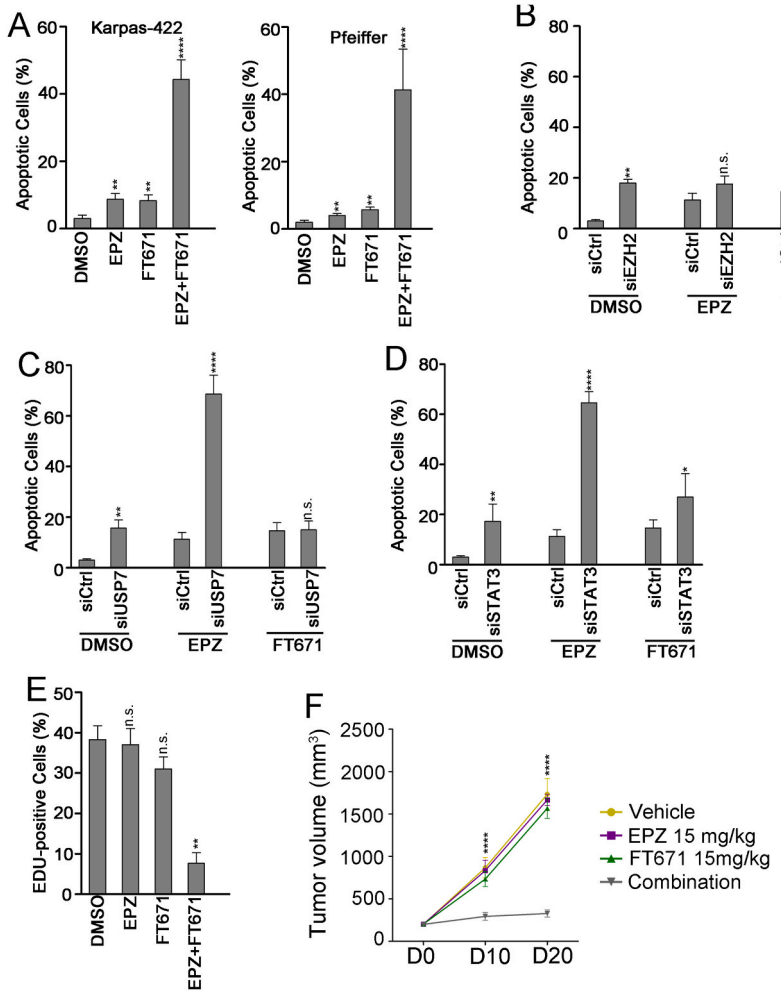

Fig. 4. Combinational perturbation of EZH2 and USP7 induces apoptosis.

A. Apoptotic cells were observed in KARPAS-422 and Pfeiffer cells treated for 4 days with DMSO, 0.4 μM EPZ, 0.4 μM FT671, or 0.4 μM EPZ+0.4 μM FT671. The percentage of apoptotic cells compared to total cells was calculated. Error bars represent standard deviation for three biological replicates. P value is from two-sided student's t-test. **p < 0.01; ****p < 0.0001.

B. Apoptotic cells were observed in control siRNA (siCtrl) or EZH2 siRNA (siEZH2) transfected KARPAS-422 cells treated for 4 days with DMSO, 0.4 μM EPZ, or 0.4 μM FT671. The percentage of apoptotic cells compared to total cells was calculated. Error bars represent standard deviation for three biological replicates. P value is from two-sided student's t-test. n.s., not significant; **p < 0.01; ***p < 0.001.

C. Apoptotic cells were observed in control siRNA (siCtrl) or USP7 siRNA (siUSP7) transfected KARPAS-422 cells treated for 4 days with DMSO, 0.4 μM EPZ, or 0.4 μM FT671. The percentage of apoptotic cells compared to total cells was calculated. Error bars represent standard deviation for three biological replicates. P value is from two-sided student's t-test. n.s., not significant; **p < 0.01; ****p < 0.0001.

D. Apoptotic cells were observed in control siRNA (siCtrl) or STAT3 siRNA (siSTAT3) transfected KARPAS-422 cells treated for 4 days with DMSO, 0.4 μM EPZ, or 0.4 μM FT671. The percentage of apoptotic cells compared to total cells was calculated. Error bars represent standard deviation for three biological replicates. P value is from two-sided student's t-test. *p < 0.05; **p < 0.01; ****p < 0.0001.

E. EDU-positive KARPAS-422 cells were observed after treated for 4 days with DMSO, 0.4 μM EPZ, or 0.4 μM FT671, or 0.4 μM EPZ+0.4 μM FT671. The percentage of EDU-positive cells compared to total cells was calculated. Error bars represent standard deviation for three biological replicates. P value is from two-sided student's t-test. n.s., not significant; **p < 0.01.

F. Tomor volume over time in KARPAS-422 xenografts. Error bars represent standard error of the mean±SEM. Mice were dosed with vehicle, EPZ 15 mg/kg, FT671 15 mg/kg, or combination of EPZ 15 mg/kg and FT671 15 mg/kg daily. P value is from two-sided student's t-test. ****p < 0.0001.

2.2. Co-inhibition of EZH2 and USP7 exhibited synergistic effect on apoptosis of KARPAS cells

Within 7 days EPZ treatment at concentration from 0.011 μM to 0.93 μM, WSU-DLCL2 cell growth was not affected, and Pfeiffer cells were mildly perturbed [26]. With another drug GSK126 treatment for 6 days at concentration from 0.018 μM to 0.143 μM KARPAS-422 cells were not affect and Pfeiffer cells were mildly perturbed at 0.072 μM-0.143 μM [27]. In summary, single inhibition of EZH2 didn't show promising in vitro DLBCL cell proliferation blockage, corresponding to modest clinical trial efficacy[[11,20,22,28]]. Upregulated STAT3 and USP7 in response to EZH2 is an implication for improving EZH2-related target therapy. STAT3 has no promising inhibitor so far [29], but USP7 has recently been shown to be selectively inhibited by FT671 [23]. We sought to test inhibition of USP7 and EZH2 with FT671 and EPZ. We tested a range of concentrations (From 0.0032 μM-10 μM) of EPZ, FT671, and combination of these two drugs with concentration ratio of 1:1 within 6 days (Fig. 3 A-X). Significant cell proliferation defect was observed with single EPZ or FT671 treatment at concentration from 2 μM-10 μM, while combinatorial use of EPZ and FT671 induced cell growth defect at lower concentration (from 0.08 μM to 10 μM for KARPAS-422 and Pfeiffer cells, from 0.4 μM to 10 μM for Toledo and Farage cells) (Fig. 3 A-X). With 0.08 μM EPZ or FT671 single treatment did not block cell proliferation, while co-inhibition lead to ~50 % (Fig. 3C) reduction of Karpas-422 cell amount on day 6. Similarly, with 0.08 μM EPZ or FT671 single treatment did not block cell proliferation, while co-inhibition lead to ~60 % (Fig. 3I) reduction of Pfeiffer cell amount on day 6.

Consistent with reduced cell proliferation rate, we observed significantly increased apoptotic cells with co-inhibition of 0.4 μM EPZ and 0.4 μM FT671 for 4 days (apoptotic cells 4 % in DMSO treated cells, 9 % in EPZ treated cells, 8 % FT671 cells, and 43 % in co-inhibition cells) (Fig. 4A). To further investigate the synergy between EZH2 and USP7 or STAT3, we performed siRNA mediated knockdown in KARPAS-422 cells to transiently deplete EZH2, USP7, and STAT3. EPZ and FT671 were used to treat these siRNA transfected cells. In EZH2 siRNA treated cells, EPZ treatment induced ~19 % apoptosis, and FT671 induces ~65 % apoptosis (Fig. 4 B). In USP7 siRNA treated cells, EPZ treatment induced ~69 % apoptosis, and FT671 induced ~15 % apoptosis (Fig. 4 C). In STAT3 siRNA treated cells, EPZ treatment induced ~68 % apoptosis, and FT671 induced ~28 % apoptosis (Fig. 4 D). These results suggest high cell death efficacy with combination of USP7 inhibition and EZH2 depletion, USP7 depletion and EZH2 inhibition, and EZH2 inhibition and STAT3 depletion. EDU labeling assay further showed that co-inhibition of EZH2 and USP7 prevented cells from entering S phase (Fig. 4E). This suggests that the co-inhibition can block DLBCL cell proliferation by inducing both apoptosis and G1 phase arrest. To further test if EPZ and FT671 can team up for cancer therapy, we performed KARPAS-422 xenograft test. Upon engraft, mice were randomized to vehicle, EPZ, FT671, and combination of these two drugs. EPZ and FT671 treatment alone did not attenuate tumor growth but combination treatment showed robust perturbation (Fig. 4F), which indicated high anti-tumor efficacy with combinational inhibition of USP7 and EZH2.

3. Discussion

To investigate resistance mechanisms, we demonstrated the upregulation of oncogene STAT3 and deubiquitylase USP7 in EZH2-inhibited DLBCL cells. STAT3 and USP7 are upregulated at both RNA and protein levels. Upregulated USP7 further stabilizes MDM2 protein, which further downregulates p53 protein level. Combinatory inhibition of EZH2 and USP7 synergistically induces proliferation defect at relatively low concentrations (0.08 μM), which suggests a new therapeutic approach by co-targeting EZH2 and USP7 for DLBCL patients.

Ubiquitously expressed genes USP7 and STAT3 were emergently marked by H3K27me3. This indicates that highly active EZH2 aberrantly targets euchromatic regions in DLBCL cells and epigenetically mediates repression of these two genes by cooperating with PRC1. Our finding suggests that EZH2, a tumorigenesis-related gene, can change transcriptional profile by abnormally establishing facultative heterochromatin at euchromatic regions.

Both STAT3 and USP7 promote cell proliferation and prevent apoptosis [[23,30–32]], and are advantageous to cancer cells' survival. STAT3 as a transcription factor targets to anti-apoptotic genes, such as Mcl-1, Survivin, and BCL2 [[30,33,34]]. Indeed, we observed ~2 foldchange for BCL2 in EZH2 inhibited KARPAS-422 cells (Fig. 1A). USP7 also prevents apoptosis by stabilizing MDM2, which further destabilizes apoptotic factor p53 [23,31]. Upregulation of these two proteins indicates that DLBCL cells tolerate EZH2 inhibition, at least in part, by STAT3 and USP7 mediated mechanisms.

Combinatory inhibition of USP7 and EZH2 shows efficacy in both EZH2 mutation-containing (Karpas-422 and Pfeiffer) and EZH2 WT DLBCL (Toledo and Farage) (Fig. 3), while the efficacy is better in EZH2 mutation-containing DLBCL (concentration starting from 0.08 μM) than in EZH2 WT DLBCL (concentration starting from 0.4 μM), which suggests that gain-of-function mutation of EZH2 contributes to the resistance to single inhibition of EZH2 but it is not the only mechanism that determines the feature. EZH2 strong expression or overexpression has been observed in B-cell lymphoma and its high expression showed positive correlation with high-grade features[[35,36]], which may indicate that wild-type EZH2 is catalytically hyperactive in DLBCL through high expression level. Thus, EZH2 WT DLBCL could also show resistance to EPZ inhibition and require co-inhibition for better therapy.

Cancer epigenetic study in DLBCL may also provide insight into other lymphomas, like mantle cell lymphoma and T cell lymphoma, since EZH2's overexpression has been implicated in these cancers [37]. The combinational targeting of EZH2 with USP7, and/or STAT3 may be a potential solution for them.

4. Methods

4.1. Cell culture and treatment

KARPAS-422 (gift from David Weinstock lab), Farage (ATCC, CCL-2630), Toledo (ATCC, CCL-2631), Pfeiffer (ATCC, CCL-2632), and WSU-DLCL2 (DSMZ, ACC575) cells, were cultured in a medium of RPMI with 20 % fetal calf serum. EZH2 inhibitor EPZ is from Med Chem Express (HY-13803). USP7 inhibitor FT671 is from Med Chem Express (HY-107985).

4.2. RNA interference

For RNA interference, LipofectamineTM RNAiMAX from Invitrogen was used for delivery of siRNA (200 nM) according to the manufacturer's instructions.

All the siRNAs used in this paper is produced by Dharmacon. The sequences are below:

siCtrl:5′-CGUACGCGGAAUACUUCGA-3′
siEZH2: 5′-GCUCUAGACAACAAACCUU-3′
siCBX2: 5′-CTGAAGCATGTTCCATTTCTA-3′
siCBX4: 5′-CGGCCTCAGAGTTCTAGTATTATAT-3′
siRING1A:5′-CCTGATCTCTAAGATCTAT-3′
siRING1B: 5′-CCTACAAAGGAGCACAAAT-3′
siUSP7: 5′-ACCCUUGGACAAUAUUCCU-3′
siSTAT3: 5′-GACGACUUUGAUUUCAAC-3′

4.3. Immunoblotting

Cells were grown in plates for 24 h, then were lysed with protein loading buffer (containing 2 % SDS) for 5 min. Lysed cell samples were boiled for 8 min at 98 °C. Boiled cell samples were run on 4–15 % gradient SDS-PAGE gel for 1 h at 100 V, and then proteins in the SDS-PAGE gel were attached to a PVDF membrane (Millipore) for transferring (1 h and 105 V). The membranes were incubated with primary antibodies and secondary antibodies (HRP-conjugated) in a TBS buffer with 5 % milk and 0.2 % Tween-20. The blotting images were obtained by chemiluminescence detection.

Antibodies used in the paper:

EZH2 (Cell Signaling Technology,5246S, WB 1:1000).
RING1A (Cell Signaling Technology,13096S, WB 1:100).
RING1B (Cell Signaling Technology,5694S, WB 1:100).
CBX2 (Proteintech, 15579-1-AP, WB 1:100).
P53 (Cell Signaling Technology,2527S, WB 1:500).
MDM2 (Cell Signaling Technology,86934S, WB 1:500).
USP7 (Cell Signaling Technology,4833T, WB 1:500).
STAT3 (Cell Signaling Technology,9139S, WB 1:200).
H3K27me3 (Cell Signaling Technology,9733S, WB 1:200).
H2AK119ub1 (Cell Signaling Technology, 8240S, WB 1:1000).
H3 (Abcam, ab1791, WB 1:1000).
H2A (Active Motif, 39945, WB 1:100).
GAPDH (Cell Signaling Technology,2118S, WB 1:200).

4.4. RT-qPCR

Total RNA from ~5 × 106 cultured cell was lysed and extracted using the RNeasy Plus kit (74134, Qiagen) and 2 μg of RNA used for reverse transcription to obtain cDNA with a cDNA synthesis kit (18090010, ThermoFisher). The cDNA samples were analyzed for gene expression levels by using real-time PCR with a QuantStudio 7 Flex Real Time qPCR machine from Applied Biosystem. Every reaction was done with 10 ng RNA-derived cDNA in a 10 μl volume of reaction. All the real time qPCR results were presented with three biological replicates. The real time qPCR.

1.95 °C for 2 min.
2.40 cycles of 95 °C for 15s, 60 °C for 15s, and 72 °C for 15 s.
3.72 °C for 1 min.

4.5. ChIP-qPCR

Ten million cells (cultured in 15 cm plates) were washed with pre-cold PBS 3 times, treated with 1 % formaldehyde (ThermoFisher Scientific) for 12 min at room temperature, which were quenched by adding glycine (125 mM in water) for 5 min at room temperature. Crosslinked cells were washed for 3 times followed by treatment of 0.05 % trypsin (Gibco) for 3 min. Hypotonic buffer (pH 7.4, Hepes-

KOH 5 mM, KCl 85 mM, NP-40 1 %, 1xProtease inhibitor cocktail from Roche) were used for the cells at 4 °C for 10 min, followed by douncing for 10 times to break cell membrane. Cell nuclei were isolated with centrifugation for 3 min at 3000g, which were further resuspended in ChIP buffer (50 mM Hepes, 1 mM EDTA, 140 mM NaCl, 0.1 % Sodium deoxycholate, 1 % Triton, and 0.5 % SDS, pH 7.9). Shearing chromatin into ~300 bp fragments using a Branson sonicator, then the samples were diluted 5-fold with dilution buffer (1 mM EDTA, 140 mM NaCl, 1 % Triton, pH 7.9, 50 mM Hepes, 0.1 % Sodium deoxycholate, no SDS). Diluted samples were transferred to a pre-cold centrifuge (13,000 rpm for 10 min). The supernatant was obtained for immunoprecipitation using 3 μg antibodies and 20 μl protein A/G beads for 3–12 h. The beads were washed: twice with wash buffer A (500 mM NaCl, 1 % Triton, 1 mM EDTA, 0.1 % Sodium deoxycholate, 0.1 % SDS, pH 7.9, 50 mM Hepes) and once with wash buffer B (250 mM LiCl, 1 % Triton, 1 mM EDTA, 0.1 % Sodium deoxycholate, pH 7.9, 50 mM Hepes, 0.5 % NP-40). The bound chromatin fragments and antibodies on beads were eluted in ChIP elution buffer (10 mM EDTA, pH 8.0, 50 mM Tris, 1 % SDS) for 5 min at 65 °C. Eluted antibody-protein-DNA complexes were treated with RNase A for RNA elimination and overnight at 65 °C for reverse crosslinking. Proteinase K was further added into the eluted and reverse crosslinked samples for digestion (1 h at 55 °C). ChIP DNA was then purified using DNA Purification Kit from QIAGEN and analyzed by qPCR. For the details of qPCR reaction please see the description in "RT-qPCR" section.

4.6. Apoptosis assay

Cells were plated in 24-well plates at a density of approximately 500,000 cells per well. Cells were trypsinized to get single cell and washed once with PBS. Annexin V/propidium iodide kit (ThermoFisher) was used to double stain cells. Cell apoptosis was measured and Annexin V-positive/propidium iodide-negative cells were counted as apoptotic cells.

4.7. Xenograft

KARPAS-422 tumors were implanted subcutaneously in NOD-SCID mice. Mice were purchased from the Jackson Laboratory and randomized to Vehicle or drugs upon engraft (tumor volume 180–220 mm3). Mice experiments protocols were approved from local authorities, and experiments were performed in accordance with relevant guidelines and regulations. Mice experiments were in accordance with ARRIVE guidelines.

Ethics statement

Animal experiments were approved by ethics committee of Institute Of Biophysics with approval number SYXK2023176.

Additional information

ChIP-seq and RNA-seq data are published and publicly available in NCBI. ChIP-seq of H3K27me3 in DLBCL is available from GSE40972. ChIP-seq of H3K27me3 in K562 is available from GSE70482. ChIP-seq of H3K27me3 in HEK293FT and HeLa is available from GSE175678. RNA-seq is available from GSE62058.

CRediT authorship contribution statement

Chenyun He: Data curation, Formal analysis, Funding acquisition, Investigation, Methodology, Project administration, Resources, Software, Validation, Visualization. **Wenbin Zhou:** Methodology. **Xiaoxia Jin:** Methodology. **Haining Zhou:** Conceptualization, Writing – original draft, Writing – review & editing, Supervision.

Declaration of competing interest

The authors declare that they have no known competing financial interests or personal relationships that could have appeared to influence the work reported in this paper.

Acknowledgements

We thank Professor David Weinstock for kindly giving KARPAS-422 cells. We thank Dr. Gongwei Wu for advice on KARPAS-422 cell culture. This work was supported by Health Committee Science Project of Nantong (WB2021045).

Appendix A. Supplementary data

Supplementary data to this article can be found online at https://doi.org/10.1016/j.heliyon.2023.e20650.

References

[1] V. Kashyap, et al., Regulation of stem cell pluripotency and differentiation involves a mutual regulatory circuit of the NANOG, OCT4, and SOX2 pluripotency transcription factors with polycomb repressive complexes and stem cell microRNAs, Stem Cell. Dev. 18 (7) (2009) 1093–1108.
[2] B. Schuettengruber, et al., Genome regulation by polycomb and trithorax: 70 Years and counting, Cell 171 (1) (2017) 34–57.
[3] X. Liu, et al., Distinct features of H3K4me3 and H3K27me3 chromatin domains in pre-implantation embryos, Nature 537 (7621) (2016) 558–562.
[4] L. Di Croce, K. Helin, Transcriptional regulation by Polycomb group proteins, Nat. Struct. Mol. Biol. 20 (10) (2013) 1147–1155.
[5] K. Basso, R. Dalla-Favera, Germinal centres and B cell lymphomagenesis, Nat. Rev. Immunol. 15 (3) (2015) 172–184.
[6] W. Beguelin, et al., EZH2 is required for germinal center formation and somatic EZH2 mutations promote lymphoid transformation, Cancer Cell 23 (5) (2013) 677–692.
[7] W. Beguelin, et al., EZH2 and BCL6 cooperate to assemble CBX8-BCOR Complex to repress bivalent promoters, mediate germinal center formation and lymphomagenesis, Cancer Cell 30 (2) (2016) 197–213.
[8] W. Beguelin, et al., Mutant EZH2 induces a pre-malignant lymphoma niche by reprogramming the immune response, Cancer Cell 37 (5) (2020) 655–673 e11.
[9] C. Bodor, et al., EZH2 mutations are frequent and represent an early event in follicular lymphoma, Blood 122 (18) (2013) 3165–3168.
[10] C. Bodor, et al., EZH2 Y641 mutations in follicular lymphoma, Leukemia 25 (4) (2011) 726–729.
[11] K.H. Kim, C.W. Roberts, Targeting EZH2 in cancer, Nat. Med. 22 (2) (2016) 128–134.
[12] M.T. McCabe, et al., Mutation of A677 in histone methyltransferase EZH2 in human B-cell lymphoma promotes hypertrimethylation of histone H3 on lysine 27 (H3K27), Proc. Natl. Acad. Sci. U. S. A. 109 (8) (2012) 2989–2994.
[13] R.D. Morin, et al., Somatic mutations altering EZH2 (Tyr641) in follicular and diffuse large B-cell lymphomas of germinal-center origin, Nat. Genet. 42 (2) (2010) 181–185.
[14] D.B. Yap, et al., Somatic mutations at EZH2 Y641 act dominantly through a mechanism of selectively altered PRC2 catalytic activity, to increase H3K27 trimethylation, Blood 117 (8) (2011) 2451–2459.
[15] M. Luo, Inhibitors of protein methyltransferases as chemical tools, Epigenomics 7 (8) (2015) 1327–1338.
[16] H.P. Visser, et al., The Polycomb group protein EZH2 is upregulated in proliferating, cultured human mantle cell lymphoma, Br. J. Haematol. 112 (4) (2001) 950–958.
[17] J. Yan, et al., EZH2 overexpression in natural killer/T-cell lymphoma confers growth advantage independently of histone methyltransferase activity, Blood 121 (22) (2013) 4512–4520.
[18] A. Italiano, et al., Tazemetostat, an EZH2 inhibitor, in relapsed or refractory B-cell non-Hodgkin lymphoma and advanced solid tumours: a first-in-human, open-label, phase 1 study, Lancet Oncol. 19 (5) (2018) 649–659.
[19] Izutsu, K., et al., Phase II study of tazemetostat for relapsed or refractory B-cell non-Hodgkin lymphoma with EZH2 mutation in Japan. Cancer Sci.. 112(9): p. 3627-3635.
[20] H. Quentmeier, et al., EZH2-activating mutation: no reliable indicator for efficacy of methyltransferase inhibitors, Leuk. Lymphoma 61 (12) (2020) 2885–2893.
[21] Gibaja, V., et al., Development of secondary mutations in wild-type and mutant EZH2 alleles cooperates to confer resistance to EZH2 inhibitors. Oncogene. 35 (5): p. 558-566.
[22] K. Izutsu, et al., Phase II study of tazemetostat for relapsed or refractory B-cell non-Hodgkin lymphoma with EZH2 mutation in Japan, Cancer Sci. 112 (9) (2021) 3627–3635.
[23] A.P. Turnbull, et al., Molecular basis of USP7 inhibition by selective small-molecule inhibitors, Nature 550 (7677) (2017) 481–486.
[24] M. Hu, et al., Structural basis of competitive recognition of p53 and MDM2 by HAUSP/USP7: implications for the regulation of the p53-MDM2 pathway, PLoS Biol. 4 (2) (2006) e27.
[25] W.D. Bradley, et al., EZH2 inhibitor efficacy in non-Hodgkin's lymphoma does not require suppression of H3K27 monomethylation, Chem. Biol. 21 (11) (2014) 1463–1475.
[26] S.K. Knutson, et al., A selective inhibitor of EZH2 blocks H3K27 methylation and kills mutant lymphoma cells, Nat. Chem. Biol. 8 (11) (2012) 890–896.
[27] M.T. McCabe, et al., EZH2 inhibition as a therapeutic strategy for lymphoma with EZH2-activating mutations, Nature 492 (7427) (2012) 108–112.
[28] F. Morschhauser, et al., Tazemetostat for patients with relapsed or refractory follicular lymphoma: an open-label, single-arm, multicentre, phase 2 trial, Lancet Oncol. 21 (11) (2020) 1433–1442.
[29] H. Yu, et al., Revisiting STAT3 signalling in cancer: new and unexpected biological functions, Nat. Rev. Cancer 14 (11) (2014) 736–746.
[30] S. Bhattacharya, R.M. Ray, L.R. Johnson, STAT3-mediated transcription of Bcl-2, Mcl-1 and c-IAP2 prevents apoptosis in polyamine-depleted cells, Biochem. J. 392 (Pt 2) (2005) 335–344.
[31] Y.H. Fan, et al., USP7 inhibitor P22077 inhibits neuroblastoma growth via inducing p53-mediated apoptosis, Cell Death Dis. 4 (2013) e867.
[32] P.A. Johnston, J.R. Grandis, STAT3 signaling: anticancer strategies and challenges, Mol. Interv. 11 (1) (2011) 18–26.
[33] P.K. Epling-Burnette, et al., Inhibition of STAT3 signaling leads to apoptosis of leukemic large granular lymphocytes and decreased Mcl-1 expression, J. Clin. Invest. 107 (3) (2001) 351–362.
[34] T. Gritsko, et al., Persistent activation of stat3 signaling induces survivin gene expression and confers resistance to apoptosis in human breast cancer cells, Clin. Cancer Res. 12 (1) (2006) 11–19.
[35] Y. Liu, et al., EZH2 overexpression in primary gastrointestinal diffuse large B-cell lymphoma and its association with the clinicopathological features, Hum. Pathol. 64 (2017) 213–221.
[36] Z. Zhou, et al., Strong expression of EZH2 and accumulation of trimethylated H3K27 in diffuse large B-cell lymphoma independent of cell of origin and EZH2 codon 641 mutation, Leuk. Lymphoma 56 (10) (2015) 2895–2901.
[37] P. Dursun, et al., Primary cervical lymphoma: report of two cases and review of the literature, Gynecol. Oncol. 98 (3) (2005) 484–489.